Microsc. Microanal. 7, 470–485, 2001
DOI: 10.1007/s10005-001-0021-3

Microscopy AND Microanalysis

In Situ Environmental Cell–Transmission Electron Microscopy Study of Microbial Reduction of Chromium(VI) Using Electron Energy Loss Spectroscopy

Tyrone L. Daulton,[1]* Brenda J. Little,[2] Kristine Lowe,[3] and Joanne Jones-Meehan[3]

[1]*Marine Geosciences Division, Naval Research Laboratory, Stennis Space Center, MS 39529*
[2]*Oceanography Division, Naval Research Laboratory, Stennis Space Center, MS 39529*
[3]*Chemistry Division, Naval Research Laboratory, Washington, DC 20375*

Abstract: Reduction of Cr(VI) by the bacterium, *Shewanella oneidensis* (previously classified *Shewanella putrefaciens* strain MR-1), was studied by absorption spectrophotometry and in situ, environmental cell–transmission electron microscopy (EC-TEM) coupled with electron energy loss spectroscopy (EELS). Bacteria from rinsed cultures were placed directly in the environmental cell of the transmission electron microscope and examined under 100 Torr pressure. Bright field EC-TEM images show two distinct populations of *S. oneidensis* in incubated cultures containing $Cr(VI)O_4^{2-}$: those that exhibit low image contrast and heavily precipitate-encrusted cells exhibiting high image contrast. Several EELS techniques were applied to determine the oxidation state of Cr associated with encrusted cells. The encrusted cells are shown to contain a reduced form of Cr in oxidation state +3 or lower. These results demonstrate the capability to determine the chemistry and valence state of reduction products associated with unfixed, hydrated bacteria in an environmental cell transmission electron microscope.

Key words: in situ transmission electron microscopy, environmental cell, electron energy loss spectroscopy, environmental cell–transmission electron microscopy, dissimilatory metal reduction, Cr(VI) reduction, bacteria

Introduction

The geochemistry and toxicity of chromium is controlled by its valence state. Chromium is a redox active 3*d* transition metal with a wide range (−2 to +6) of possible oxidation states, however, only two are stable. Thermodynamic calculations predict hexavalent Cr(VI) is energetically favored for oxic conditions and trivalent Cr(III) predominates under anoxic or suboxic conditions. Both Cr(VI) and Cr(III) have been detected in suboxic groundwater (Bartlett and James, 1988), seawater (Mugo and Orians, 1993), and estuarine water (Cranston and Murray, 1980).

The two stable oxidation states of Cr have markedly different properties. Chromium(VI) readily binds to oxygen and therefore can exist as highly soluble chromate (CrO_4^{2-}), hydrochromate ($HCrO_4^-$), and dichromate ($Cr_2O_7^{2-}$) anions, representing the three main Cr(VI) species in solution. Their relative distribution is reportedly sensitive to solution pH (Tandon et al., 1984; Brito et al., 1997). In very acidic

Received January 24, 2001; accepted June 13, 2001.
*Corresponding author

solutions, two other forms have been detected, $Cr_3O_{10}^{2-}$ and $Cr_4O_{13}^{2-}$ (Cieslak-Golonka, 1991). Oxo-anionic Cr(VI) species have an absorption affinity for certain proton-specific mineral surfaces, however, adsorption is limited in natural aqueous systems by competing anions like sulfate (Zachara et al., 1987). Toxicity to plants and animals is well established for Cr(VI) species which act as carcinogens, mutagens, and teratogens (see Cieslak-Golonka, 1995). The structural similarly of CrO_4^{2-} ions to biologically important inorganic anions, such as SO_4^{2-} and PO_4^{3-}, is likely responsible for its ability to readily transverse cell membranes, via the sulfate transport system, and be incorporated into cells. The high mobility (bioavailability) and toxicity of Cr(VI) make it a particular environmental concern.

In comparison, Cr(III) exists in solution as a cation, $Cr^{3+}(aq)$, and hydroxo complexes (e.g., $Cr(OH)_n^{(3-n)+}$). Less mobile than Cr(VI), Cr(III) has strong affinity for particle surfaces (Baes and Mesmer, 1976; Holdway, 1988) and forms low-solubility solid phases such as $Cr(OH)_3$ and $(Cr, Fe)(OH)_3$ (Rai et al., 1987). Chromium(III) has a low toxicity, in part, because its bioavailability is limited by its low solubility and its tendency to form strong complexes with organics and hydroxo complexes. Furthermore, as opposed to Cr(VI), trace amounts of Cr(III) are necessary for normal development of animals (Hamilton and Wetterhahn, 1987; Dubois and Belleville, 1991; Katz, 1991).

Hexavalent Cr(VI) can be readily reduced to the trivalent state by Fe^{2+} (Sedlak and Chan, 1997; Pettine et al., 1998b), S^{2-} (Pettine et al., 1994, 1998a), UV photocatalysts (see Ku and Jung, 2001), organic compounds (Deng and Stone, 1996a,b), some wetland plants (Lytle et al., 1998), and several species of microorganisms (for a review, see Lovley, 1993). The associated mechanisms of Cr(VI) reduction are technologically and biologically important because they convert a toxic, mobile element into a less toxic, immobile form. It is essential to understand these processes since reduction products, as well as their stability, are dependent on specific redox mechanisms and the environment.

The role of microbiological reduction of Cr(VI) in natural aqueous systems is receiving progressively more attention as more metal-reducing bacteria are identified. In aerobic environments, bacteria play the predominant role in reducing Cr(VI) to Cr(III) (Fendorf et al., 2000). Little is known about the biochemical or molecular mechanisms underlying bacterial metal reduction. Conventional transmission electron microscopy (TEM) studies of microbial reduction of metals have provided some information. However, they are limited because the techniques of fixation, dehydration, embedding, and microtoming, necessary to prepare thin specimens, are known to alter delicate cellular structures as well as the extracellular polymers excreted by bacteria. Bacterial extracellular polymeric substances (EPS) are thought to assist in respiration, surface attachment, and nutrient uptake, and to provide protection from the environment (Vandevivere and Kirchman, 1993; Decho 2000). Although the composition of these excretions varies with microorganism and environment, they predominately contain anionic mucopolysaccharides in addition to some proteinaceous materials. There are many chemically active sites in the net negatively charged, extracellular-polysaccharide matrix which have been shown to complex inorganic cations as well as absorb organic molecules (Characklis and Marshall, 1990). Fixation and dehydration preserve some of the structure of EPS encapsulated bacteria, but buffer and organic solvent washes remove extracellular polymers as well as soluble ions from extracellular and intracellular sources. Furthermore, dehydration causes extracellular biopolymers to collapse into a filamentous, web-like network. Valuable data on dehydration artifacts related to microorganisms has been provided by environmental scanning electron microscopy (ESEM) (Little et al., 1991). Environmental cell (EC) techniques, particularly when coupled with TEM, are advantageous because unfixed, EPS encapsulated hydrated bacteria can be examined at high spatial resolution.

We report preliminary in situ EC-TEM results of our study on Cr(VI) reduction by *Shewanella oneidensis,* a gram-negative, facultative bacterium, capable of respiring aerobically and anaerobically using a variety of compounds, including: O_2, Fe(III), Mn(IV), NO_2^-, NO_3^-, SO_2, sulfite (SO_3^{2-}), thiosulfate ($S_2O_3^{2-}$), tetrathionate ($S_4O_6^{2-}$), trimethylamine N-oxide, fumarate, glycine, U(VI), and Cr(VI) as terminal electron acceptors (see Myers and Nealson, 1988a,b; Lovley et al., 1991). *S. oneidensis,* a member of the γ-subclass of *Proteobacteria,* has been isolated from lascustrine and marine environments. This species is of particular interest because its total genome is currently being sequenced by The Institute of Genomic Research in Bethesda, MD. In this work, *S. oneidensis* was grown in a synthetic medium containing CrO_4^{2-} anions. The reduction of Cr(VI) in these cultures was measured spectrophotometrically using colorimetric techniques. Microanalysis of individual bacteria and their associated reduction products was performed by EC-TEM.

Materials and Methods

Bacterial Cultures

The bacteria presently classified as *S. oneidensis* (Venkateswaran et al., 1999), previously classified *Shewanella putrefaciens* strain MR-1 (MacDonell and Colwell, 1985), and before that classified in a different genus as *Alteromonas putrefaciens* (Lee et al., 1977), were isolated from the anaerobic zone of Mn-rich sediments in Oneida Lake, NY (Myers and Nealson, 1988b). The bacteria were initially grown under aerobic conditions at 30°C for 5 days (spectrophotometry study) and 18 to 24 hr (EC-TEM study) in LB Broth (Difco Laboratories, Detroit, MI) with continuous agitation. Samples of 5 mL of the initial culture were transferred to flasks containing 250 mL of an anaerobic growth medium (adapted from Myers and Nealson, 1988a). The growth medium consisted of autoclaved dH_2O, a salt component (9.0 mM $(NH_4)_2SO_4$, 5.7 mM $K_2HPO_4{\cdot}3H_2O$, 3.3 mM KH_2PO_4, and 2.0 mM $NaHCO_3$), and a trace metal component (70 μM $Na_2EDTA{\cdot}2H_2O$, 60 μM H_3BO_3, 10 μM NaCl, 6 μM $FeSO_4{\cdot}7H_2O$, 5 μM $CoCl_2{\cdot}6H_2O$, 5 μM $Ni(NH_4)(SO_4)_2{\cdot}6H_2O$, 4.0 μM $Na_2MoO_4{\cdot}2H_2O$, 1.5 μM Na_2SeO_4 (anhyd), 1.3 μM $MnSO_4{\cdot}H_2O$, 1.0 μM $ZnSO_4{\cdot}7H_2O$, and 0.2 μM $CuSO_4{\cdot}5H_2O$). The following amino acids and vitamins were present in the medium: 10^{-4} mg-L^{-1} casamino acids, 10^{-3} mg-L^{-1} vitamin B_1 (Thiamine), 0.02 mg-L^{-1} L-arginine HCl, 0.02 mg-L^{-1} L-glutamic acid, 0.02 mg-L^{-1} L-glutamine, and 0.04 mg-L^{-1} L-serine. The following co-factors were present in the medium: 1 mM $MgSO_4{\cdot}7H_2O$ and 0.5 mM $CaCl_2{\cdot}2H_2O$. For a carbon source, the medium contained 18 mM sodium lactate.

In a reduction rate experiment, the culture was purged with N_2 for 20 min with out-gassing to remove dissolved O_2. Cells were treated with antibiotic chloramphenicol (final concentration = 100 μg/ml) to stop cell division and maintain a constant cell population. An electron acceptor, K_2CrO_4, was added to the anaerobic medium to introduce Cr(VI) in the form of 170 μM CrO_4^{2-}. Subsamples were withdrawn every 5 min and reacted with diphenylcarbazide reagent in acid solutions. A Hach DR-4000V spectrophotometer (Hach Co., Loveland, CO) was then used to determine Cr(VI) concentration by measuring absorbance at 540 nm by the stoichiometric oxidation products, as described in *Standard Methods for the Examination of Water and Wastewater* (Clesceri et al., 1999).

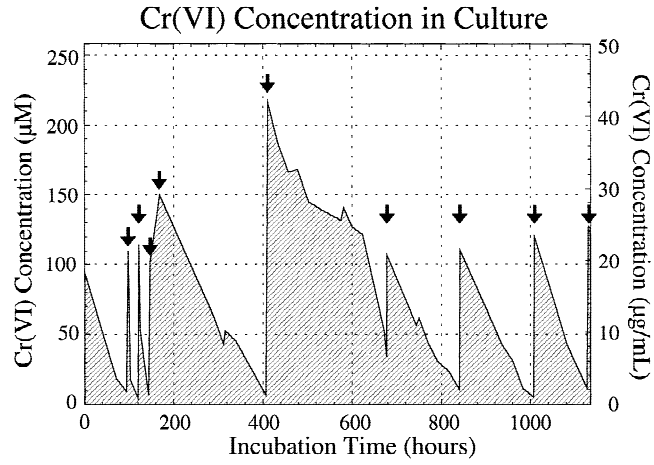

Figure 1. Chromium(VI) concentration in the *Shewanella oneidensis* culture as a function of time measured by colorimetric assay using spectrophotometry. An elevated Cr(VI) concentration was maintained by quasi-periodic spiking (indicated by the arrows).

For the EC-TEM studies, cells were grown anaerobically in the defined medium with K_2CrO_4 added to introduce Cr(VI) in the form of 100 μM CrO_4^{2-}. At the onset of the experiment, the initial pH of the medium was approximately 6.7. Cultures were incubated at room temperature on a bench-top stir plate attached to a N_2 gas line. At predetermined intervals, the culture was aseptically sampled and analyzed for Cr(VI) concentration by a Thermo Spectronic, Spectronic 20 spectrometer (Thermo Spectronic, Rochester, NY) using the diphenylcarbazide method. An elevated Cr(VI) concentration was maintained by respiking the culture with K_2CrO_4 after 96, 120, 144, 168, 408, 672, 840, 1008, and 1128 hr (Fig. 1). A total of 0.275 moles K_2CrO_4 was added to the culture. After 51 days of incubation, 200 mL of culture were removed from the reactor, sealed in a test tube, and shipped for EC-TEM examination. Bacteria were examined 53 days after initial inoculation into the culture medium. The sample was centrifuged, supernatant removed, and the pellet rinsed with distilled water to remove trace salts. An aliquot containing suspended bacteria was loaded into the EC-specimen holder and examined under an atmosphere at 100 Torr of air saturated with water vapor.

Environmental Cell–Transmission Electron Microscopy

A JEOL JEM-3010 transmission electron microscope (JEOL USA Inc., Peabody, MA) operating at 300 keV with a LaB_6

filament was used in this study. This instrument is equipped with an energy dispersive X-ray spectroscopy (EDXS) system, a Gatan imaging filter (GIF200) (Gatan Inc., Warrendale, PA) capable of electron energy loss spectroscopy (EELS), and a JEOL EC system with interchangeable EC-specimen holders. Two EC-holders were available: a two-line gas EC holder and a four-line gas/liquid EC holder (Fig. 2). These holders are connected to the EC system by flexible, stainless steel lines (see Fig. 3). Both in situ holders are capable of circulating dry or water-saturated gas through the specimen chamber using two lines for gas circulation. The gas can be saturated with water vapor by bubbling gas through a heated water reservoir, enabling the examination of hydrated specimens. The four-line holder has two additional lines which can be used to independently inject several microliters of two different liquids.

The EC used in this study is of the closed cell type, and was developed by Dr. Fukami of Nihon University in Japan (Fukami et al., 1991). Unlike EC systems based on the principle of differential pumping, closed-cell EC systems require no modification to the transmission electron microscope. Confinement of the pressurized environment within the EC is achieved with electron-transparent windows. Since the EC is self-contained within the specimen holder, the transmission electron microscope can still be used for conventional TEM without compromising resolution and analytical capabilities.

Windows for the EC were fabricated from 15–20-nm thick amorphous carbon (a-C) films which cover seven hexagonally arrayed, 0.15-mm apertures on a 3.5-mm diameter Cu disk. Prior to use, windowed grids were tested to withstand a pressure differential of 250 Torr for 1 min. A computer controls the EC system, facilitating insertion and removal of EC holders from the microscope column without breaching the delicate windows. The EC was operated at 100 Torr with room air saturated with water vapor circulating through the cell at a rate of 2 Torr-liter/min. Specimens were supported on the lower, a-C film window. The microscope was also equipped with conventional single- and double-tilt specimen holders for conventional TEM.

The following conditions were used for the collection of EELS spectra under EC-TEM and TEM conditions: an illumination angle 2α = 4–10 mrad, a collection angle of 2β = 10.8 mrad, a 2 mm entrance aperture, and an energy dispersion of 0.1 eV/channel. Low-loss spectra were acquired with an integration time of 0.128 sec and core-loss spectra between 0.512 and 1.02 sec. For each acquisition, 10 spectra were summed. Spectra were collected in diffraction

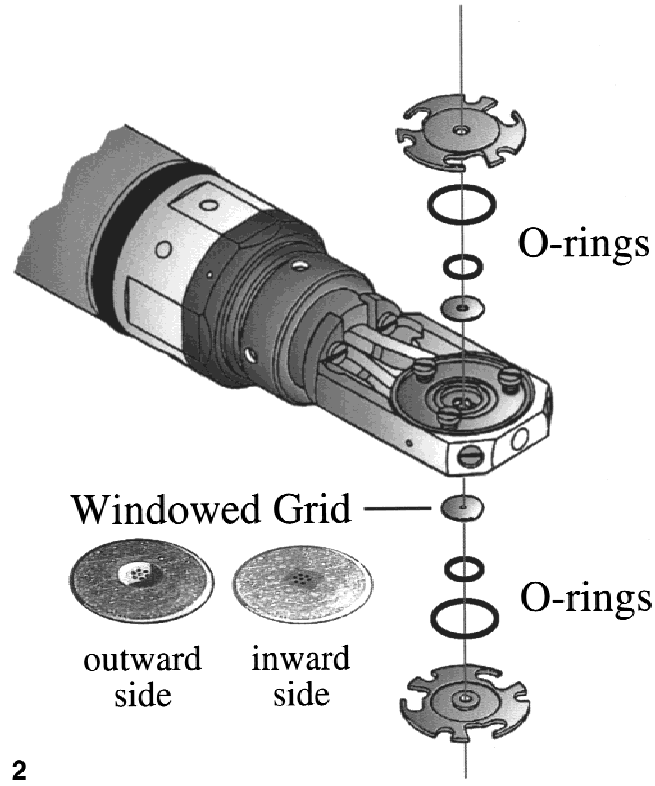

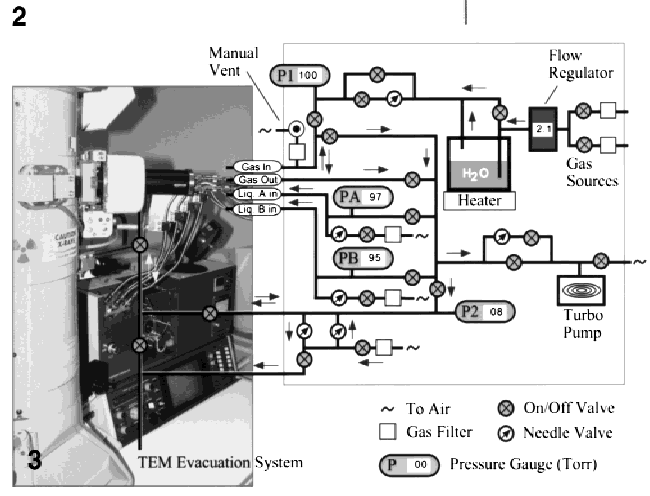

Figure 2. Schematic illustration of the specimen chamber for the four-line environmental cell (EC) specimen holder used in this study.

Figure 3. Schematic illustration of the EC control system. TEM, transmission electron microscopy.

mode of the transmission electron microscope (i.e., image coupling to the EELS spectrometer) and were corrected for dark current and channel-to-channel gain variation of the charge coupled device (CCD) detector.

Energy calibration of the core-loss regime and measurement of energy drift during data acquisition were performed by collecting zero-loss spectra before and following collection of core-loss spectra. The energy of the core-loss

spectra was calibrated using the average position of the two zero-loss peaks. The error in the energy calibration corresponded to the energy drift of the zero-loss peaks. In addition, a C-K edge spectrum was acquired immediately following spectrum collection from the O-K/Cr-L core-loss regime. The position of the C-K (*1s*) peak at 284.9 ± 0.1 eV (arising from transitions to the π^* molecular orbital) from the TEM a-C support film was used to evaluate the energy calibration. Only sets of spectra whose energy calibration was consistent with the position of the C-K,π^* peak were used. Either the pre-O-K edge background or the pre-Cr-L edge background (depending on the analysis to be performed) was subtracted from core-loss spectra using a power law, and plural inelastic scattering was removed by Fourier deconvolution methods (e.g., see Egerton, 1996).

Hydrated bacteria were analyzed by EELS through the EC-holder, while Cr oxidation state standards were analyzed using conventional TEM holders. Standards were produced by placing high purity $Cr(II)F_2$, Cr(II)Se, $Cr(III)Cl_3$, $Cr(III)_2O_3$, $KCr(III)(SO_4)_2 \cdot 12H_2O$, and $K_2Cr(VI)O_4$ powders directly on Cu TEM grids coated with holey a-C. Once the standard was prepared, it was immediately examined. For each standard, 20 individual grains were analyzed by EELS. Their results were averaged together and the errors reported for the mean represent the standard error of those measurements.

Results and Discussion

Absorption Spectrophotometry of Cultures

The results of comparative spectrophotometry measurements of Cr(VI) reduction by *S. oneidensis* and a control are shown in Figure 4. Each data point in Figure 4 represents the mean of three replicate measurements. The error bar is the standard error of the mean. No significant Cr(VI) reduction is observed for the autoclaved control, illustrating that abiotic mechanisms can largely be ignored. Considerable reduction occurs in growth media inoculated with *S. oneidensis* indicating biological processes are the predominant mechanisms for Cr(VI) reduction in these cultures. Bacterial reduction of transition metals involves many poorly understood reactions such as electron transport, anion transport through cellular membranes, anion complexation, and biological redox reactions. Additional factors influencing bacterial reduction include finite reduction capacity resulting from the termination of metabolic activity due to Cr(VI) toxicity or mutation arising from DNA damage.

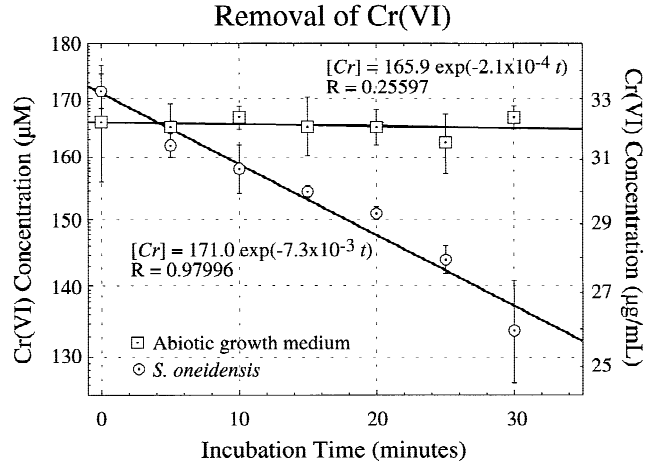

Figure 4. Relative rates of Cr(VI) reduction in *S. oneidensis* inoculated and cell-free, autoclaved growth medium. A colorimetric assay using spectrophotometry was used to measure Cr(VI) concentration. For comparative characterization, both data sets were least squares fit to an exponential decay function.

Despite the complexity, the reduction of Cr(VI) by *S. oneidensis* follows, to a good approximation, the general, first-order rate expression $-d[Cr(VI)]/dt = k_1[Cr(VI)]$, where k_1 is the rate constant. Therefore, k_1, is a useful quantity for comparative characterization of the Cr(VI) reduction in the cultures. Kinetic models of enzymatic Cr(VI) reduction based on Monod kinetics, which are more detailed, have been proposed (Wang and Shen, 1997).

Imaging Bacteria by EC-TEM

Examination of *S. oneidensis* by EC-TEM at 100 Torr, under a circulation of air saturated with water vapor, shows rod-shaped morphology typical of this polarly flagellated and non-spore-forming species (Fig. 5). The micrographs demonstrate that bacterial membranes are intact and do not show evidence of rupture from partial decompression. Cells remain plump/hydrated while the EPS retain moisture and appear as a continuous capsule surrounding the cells. Specimen artifacts typical of conventional TEM specimen preparation are avoided. However, damage to the cells is observed within minutes of electron-beam exposure. This degradation can arise from the primary destruction of weak Van der Waals biomolecular bonds when ionizing energy is transferred by inelastic electron scattering or from secondary reactions with irradiation formed free radicals. In this work, bacteria were examined following reduction of Cr(VI), therefore, it was not necessary to maintain the bacteria in a

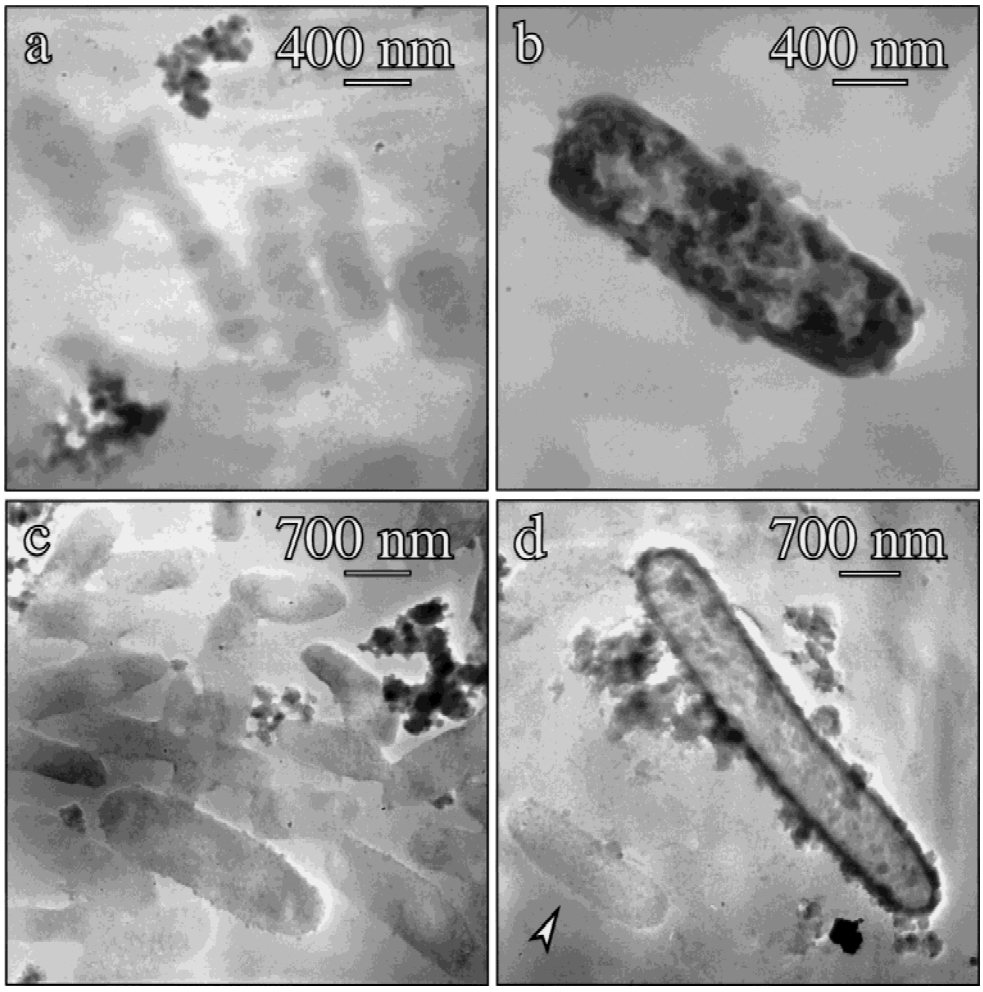

Figure 5. *S. oneidensis* imaged in the EC at 100 Torr: bacteria exhibiting low contrast in bright field EC-TEM imaging **(a, c),** and bacteria encrusted/impregnated with electron dense particulates **(b, d).** The arrowhead in panel d points to a low contrast bacterium in the same field of view as a bacterium with electron dense particulates, illustrating the dramatic contrast difference. The low-contrast, diffuse background, best seen in panel a, represents the extracellular polymeric substances that surround the cells.

viable state during imaging and irradiation damage was largely not a concern. However, low-dose techniques have been successfully applied in EC-TEM studies of Adenosine Tri-Phosphate (ATP)-induced myosin head movement in living muscle thick filaments (Sugi et al., 1997).

Direct imaging by EC-TEM reveals two distinct populations of *S. oneidensis* in the cultures: bacteria exhibiting low image contrast (Fig. 5a,c) and bacteria encrusted/impregnated with electron-dense particles (Fig. 5b,d). Since the bacteria are not imaged in thin-section, the particles associated with the high-contrast bacteria could be intracellular, on the outer-cell membrane, or both. The precipitates range in size between 10 and 200 nm, and selected area diffraction indicates the grains are predominantly amorphous in structure. It is clear that there are particles which encrust the outer-cell membrane as some of these particles can be seen protruding from the perimeter of the bacteria (Fig. 5b,d). In comparison, a lower resolution ESEM image of an *S. oneidensis* culture is shown in Figure 6. The technique of ESEM is sensitive to surface topology, suggesting the features imaged on the bacteria are precipitates encrusting their surface. Particles on the outer cell membrane will obstruct imaging of intracellular structures by EC-TEM. Intracellular precipitates may also be present, however, confirmation would require examination of the bacteria in ultrathin section.

Further examination of the bright field EC-TEM images of the encrusted bacteria shows that their gram-negative, cell envelope (consisting of an outer membrane separated from an inner cytoplasmic membrane by a periplasmic space containing the peptidoglycan cell wall) is electron dense (Fig. 5d). This is most clearly evident by the 30–49-nm thick electron-dense layer defining the two-dimensional, projected perimeter of the bacteria. The cell envelope appears darkest along the perimeter because this is where the electron path length is the greatest through the cell envelope. This increase in contrast over non-encrusted bacteria, cannot be explained by a partial dehydration ef-

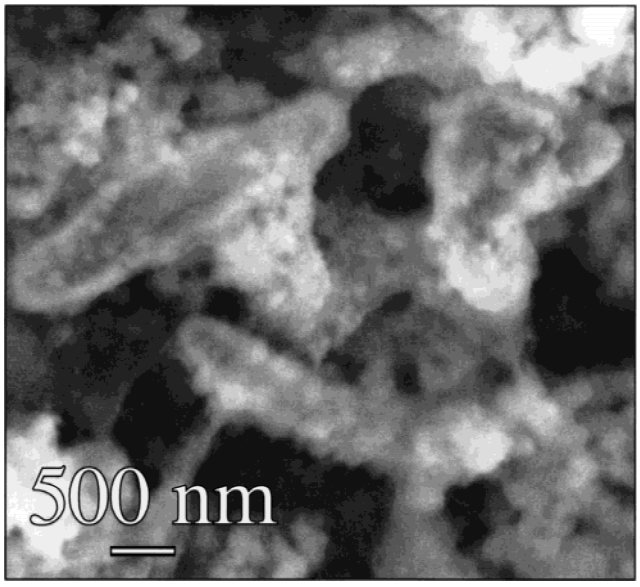

Figure 6. *S. oneidensis* imaged by environmental scanning electron microscopy (ESEM) at 4.0 Torr. The specimen is uncoated and imaged in a hydrated state by an ElectroScan Model E3 environmental scanning electron microscope (FEI, Hillsboro, OR) operating at 20 keV.

fect, i.e., more mass at the cell envelope than in the interior of the cell. Bacteria deposited on an a-C coated TEM grid and examined under high vacuum of the TEM show ruptured membranes and obvious dehydration damage, however, the cell envelopes of non-encrusted cells produce very low image contrast as compared to encrusted bacteria. Therefore, the increase in contrast indicates that the cell envelope is saturated with absorbed elements of heavy mass, for instance Cr. It is possible that cell envelope is electron dense because of the presence of bound Ca, however, only those bacteria encrusted with precipitates (shown Cr-rich in the next section) exhibit electron dense cell envelopes. Therefore, the binding of heavy elements in the cell envelope appears associated with Cr reduction.

Bioaccumulation of precipitates by bacteria has been shown in previous conventional TEM studies. A consortium of sulfate-reducing bacteria, cultured in an anaerobic medium containing Cr(VI) ions, accumulated Cr-rich amorphous precipitates presumably on the bacterial surfaces (Fude et al., 1994). Similarly, an *Aeromonas* sp. became electron-dense after removing Cr(VI) (originally in form of CrO_4^{2-}) from culture media (Hill and Cowley, 1986). In that work, it was inferred that reduced chromium accumulated as intracellular electron-dense bodies. Electron-dense particles were also associated with *Pseudomonas aeruginosa* after cell incubation in a CrO_4^{2-} containing medium (Marques et al., 1982). Evidence that precipitates were intracellular was suggested by the inability to remove the precipitates from the cells by washing with 1 mM ethylene diamine tetra-acetic acid (EDTA) adjusted to pH 2 with H_2SO_4. For prokaryotic (such as bacteria) and eukaryotic cells, Cr(VI) can pass through the cellular membrane and reduce to Cr(III) in the cytoplasm. Eukaryotic cells can additionally reduce Cr(VI) in mitochondria and nuclei (Ohtake et al., 1990). Trivalent Cr(III) is impermeable to biological membranes so that Cr(III) generated inside the cell binds to protein and interacts with nucleic acids. Unfortunately, no oxidation state measurements were performed in any of the previous conventional TEM studies. In those studies, the electron-dense particulates associated with the cells were assumed to be products of Cr bioreduction.

Chemical Analysis of Bacteria by EELS

In this work, the chemistry and oxidation state of the particulates associated with *S. oneidensis* were analyzed by EC-TEM using EELS. Techniques using EELS were developed to determine the oxidation state of transition metal atoms at high spatial resolution (e.g., see Krishnan, 1990; Paterson and Krivanek, 1990; Cressey et al., 1993; van Aken et al., 1998) and have been applied to produce maps of oxidation state using energy filtered imaging (Wang et al., 1999). Basically, these techniques compare the differences in fine structure of $L_{2,3}$ absorption edges of metals in standards of known oxidation state. The $L_{2,3}$ absorption edges are produced predominately by excited electron dipole transitions between the core $2p_{3/2}$ and $2p_{1/2}$ spin-orbit split levels to unoccupied *d* levels. Two edges arise from transitions from the $2p_{1/2}(j = 1/2)$ state (producing the L_2 edge) and transitions from the $2p_{3/2}(j = 3/2)$ state (producing the L_3 edge). The parameter *j* is total angular momentum equal to the sum of the spin quantum number, *s,* and orbital angular momentum, *l.* Spectra of different $3d^n$ (or $4d^n$) configurations differ and can be used to identify the valency (related to the number of holes in the *d* level) of a transition metal. For example, tetrahedral Cr(VI) has an empty *d* orbital ($3d^0$ configuration) and octahedral Cr(III) has a $3d^3$ configuration. Dipole selection rules (in particular, $\Delta l = \pm 1$) restrict transitions from the L-shell core $2s_{1/2}$ level to only the *p* state. Consequently, an L_1 edge is produced by $2s_{1/2}(j = 1/2)$ transitions to the 3*p* state, but this edge is of little use to oxidation state determination because there are few unfilled *p* states in the conduction band of transition metals. Fur-

thermore, L_1 edges have broad-weak peaks because *p* states are usually filled and are more spread out in energy than *d* states. Consequently, L_1 edges are often masked by the $L_{2,3}$ post-edge structure.

The fine structure of $L_{2,3}$ lines is very sensitive to the local electronic structure of a metal atom and consequently to the valence state, in addition to atom coordination, spin-orbit interactions, and crystal field splitting. Atomic coulomb repulsion and exchange effects are also important. Spectra can vary in the position, shape, and relative intensity of the $L_{2,3}$ absorption edges. Techniques used to determine mixed/single valence states involve analysis of the following: (a) the position of the $L_{2,3}$ absorption edges, which depends on the screening of the nuclear field of a metal atom by the presence of valence-electron charge; absorption edges generally shift to higher energy with increased oxidation state (see Table 1); (b) the ratio of the $I(L_3)/I(L_2)$ integrated-peak intensity (henceforth abbreviated L_3/L_2) which depends on the number of electrons in the final (4*d* or 4*f*) state; white-line ratios generally decrease with increased oxidation state (e.g., van Aken et al., 1998); and (c) least squares fits of summed spectra of standards or calculations to the shape of $L_{2,3}$ absorption edges (e.g., Cressey et al., 1993). Furthermore, the total $L_{2,3}$ absorption edge (or white line) intensity, normalized to the post L-edge continuum, has been used to determine the *d*-electron occupancies in transition metals (e.g., Pearson et al., 1993). However, L_3/L_2 peak ratios have been shown to be more sensitive to valence state than the normalized white line intensities by energy-filtered imaging (Wang et al., 1999).

Two EELS techniques are applied to provide information on oxidation state of Cr associated with hydrated and EPS encapsulated bacteria examined in the EC. Oxidation state is determined by chemical shift of $L_{2,3}$ edges and the ratio of L_3/L_2, integrated-peak intensities. In the first technique, L_3 edges are more suitable for measuring chemical shift than L_2 edges because their intrinsic line widths are narrower and better defined. The extra broadening of the L_2 threshold peak results from the shorter lifetime of the associated $p_{1/2}$ excited state, a consequence of the Heisenberg uncertainty principle. The $p_{1/2}$ state can decay by an extra Coster-Kronig Auger decay channel in which an electron can fall back to a $p_{3/2}$ hole with the simultaneous ejection of a *d* electron. This channel is not available for the excited state associated with the L_3 edge (e.g., see Zaanen and Sawatzky, 1986). Hence, the lifetimes of L_2 peaks are shorter than L_3 peaks.

The chemical shift technique is more straightforward, and provided energy calibrations are correctly done, previously published results on well-characterized standards can be readily used. However, this technique cannot be used for quantitative determination of mixed oxidation states because the shift in absorption edges is small (e.g., ≈2 eV between Cr(VI) and Cr(III)) in comparison to typical peak widths (i.e., EELS resolution). On the other hand, the L_3/L_2 intensity ratio technique can be quantitatively applied to materials with mixed oxidation states. However, it is sensitive to analysis conditions such as the subtraction of background intensity due to transitions to unoccupied states in the continuum, as well as peak integration widths. These details can vary among researchers. Since it is necessary to analyze standards and unknowns using identical procedures, published L_3/L_2 peak ratio results are of limited use.

An example of an EC-TEM image of *S. oneidensis* encrusted with electron dense precipitates is shown in Figure 7 along with EELS low-loss and core-loss spectra from the bacterium. Analysis of the L-edge spectra by EELS requires significantly higher electron doses than during imaging. In some cases, the cell envelope is ruptured during analysis with potential mass loss. Nevertheless, if an element is detected it certainly must be associated with the bacteria, particularly when absent in the surrounding medium.

Spectra collected in the EC can contain large plural scattering effects that Fourier deconvolution might not completely remove due to finite collection angle of electrons. Although, plural scattering broadens core-loss features above threshold, the core-loss intensity immediately above threshold represents only single scattering events. Plural scattering will not displace ionization thresholds, and threshold peaks will not shift significantly. Core-edge signal will increase linearly with thickness, however, plural scattering will cause the continuum background to increase at a greater rate (Egerton et al., 1991). Additionally, plural scattering will cause edge signal to decrease from subsequent plasmon scattering of core-loss electrons. Therefore, plural scattering will reduce the visibility of an edge and the edge jump ratio, (S+B)/B, where S is the signal and B is the background. Nonetheless, if the edge is visible with a defined peak, the chemical shift of L-edges can be accurately measured. However, measurement of L_3/L_2 peak ratios are dependent on the jump ratio and accurate background subtraction. In the presence of plural scattering, larger relative errors in the measurements of L_3/L_2 peak ratios would result in comparison to measurements of peak positions.

In the EELS spectrum of *S. oneidensis* (Fig. 7b), a strong O-K edge signal produced by O *1s* transitions is observed in

Table 1. Cr-L_3 ($2p_{3/2}$) and Cr-L_2 ($2p_{1/2}$) Adsorption-Edges: XPS Binding Energies and EELS L-Edge Peak Positions

Compound	Formal valence	Cr-L_3 ($2p_{3/2}$) (eV)	Cr-L_2 ($2p_{1/2}$) (eV)	Technique	Reference
Cr	0	573.8	583.0	XPS	Allen et al., 1976
		574.1		XPS	Moffat et al., 1995
		574.1	583.5	XPS	Asami and Hashimoto, 1977
		574.3[a]	582.8[a]	EELS	Fink et al., 1985[a]
		576.5 ± 1.0	585.0 ± 1.0	EELS	Leapman et al., 1982[b]
CrP	0	574.2		XPS	Moffat et al., 1995
$Cr(CO)_6$	0	577.6	586.3	XPS	Allen et al., 1976
CrF_2	II	574.2 ± 0.1	583.5 ± 0.1	EELS	This study
CrSe	II	574.2 ± 0.1	583.1 ± 0.1	EELS	This study
$CrCl_3$	III	574.9 ± 0.1	583.4 ± 0.1	EELS	This study
		576.4	587.4	XPS	Allen et al., 1976
$CuCrO_2$	III	576.4 ± 0.2	586.2 ± 0.2	XPS	Allen et al., 1973,[c] 1976
$NaCrO_2$	III	577.0 ± 0.2	586.9 ± 0.2	XPS	Allen et al., 1973,[c] 1976
Cr_2O_3	III	575.9 ± 0.1	584.3 ± 0.1	EELS	This study
		576.5	586.0	XPS	Asami and Hashimoto, 1977
		576.6–576.8		XPS	Moffat et al., 1995
		576.8 ± 0.2	586.2 ± 0.2	XPS	Allen et al., 1973,[c] 1976
		576.8	584.8	EELS	Krivanek and Paterson, 1990
		576.8	586.7	XPS	Ikemoto et al., 1976
		577.9 ± 1.0	585.8 ± 1.0	EELS	Leapman et al., 1982[b]
$FeCr_2O_4$	III	576.0	584.0	XPS	Kendelewicz et al., 1999
$KCr(SO_4)_2 \cdot 12H_2O$	III	576.0 ± 0.1	584.5 ± 0.1	EELS	This study
		581.0	590.5	XPS	Allen et al., 1973,[c] 1976
$LaCrO_3$	III	576.1 ± 0.09	585.8 ± 0.05	XPS	Konno et al., 1992
$LiCrO_2$	III	577.0 ± 0.2	586.8 ± 0.2	XPS	Allen et al., 1973,[c] 1976
CrOOH	III	577.0	586.9	XPS	Ikemoto et al., 1976
$Cr(OH)_3 \cdot 0.4H_2O$	III	577.0	586.4	XPS	Asami and Hashimoto, 1977
		577.1		XPS	Moffat et al., 1995
CrP	III	577.4		XPS	Moffat et al., 1995
$CrCl_3 \cdot 6H_2O$	III	577.5		XPS	Moffat et al., 1995
$CrPO_4$	III	577.8		XPS	Moffat et al., 1995
$CrBO_3$	III	578.0		XPS	Moffat et al., 1995
$Cr_2(SO_4) \cdot 15H_2O$	III	578.6		XPS	Moffat et al., 1995
CrO_2	IV	576.3	586.0	XPS	Ikemoto et al., 1976
$LaCrO_4$	V	578.8 ± 0.21	588.0 ± 0.22	XPS	Konno et al., 1992
CrO_3	VI	578.3 ± 0.2	587.0 ± 0.02	XPS	Allen et al., 1973[b]
		579.1	588.3	XPS	Asami and Hashimoto, 1977
$CaCrO_4$	VI	578.9 ± 0.2	588.1 ± 0.2	XPS	Allen et al., 1973,[c] 1976
$BaCrO_4$	VI	579.1 ± 0.2	588.4 ± 0.2	XPS	Allen et al., 1973,[c] 1976
$K_2Cr_2O_7$	VI	579.4 ± 0.2	588.8 ± 0.2	XPS	Allen et al., 1973,[c] 1976
		579.8	589.1	XPS	Ikemoto et al., 1976
$Na_2Cr_2O_7$	VI	579.4 ± 0.2	588.5 ± 0.2	XPS	Allen et al., 1973,[c] 1976
$Rb_2Cr_2O_7$	VI	579.4 ± 0.2	588.7 ± 0.2	XPS	Allen et al., 1973,[c] 1976
$Cs_2Cr_2O_7$	VI	579.5 ± 0.2	588.7 ± 0.2	XPS	Allen et al., 1973,[c] 1976
$SrCrO_4$	VI	579.6 ± 0.2	588.6 ± 0.2	XPS	Allen et al., 1973,[c] 1976
K_2CrO_4	VI	578.6 ± 0.1	587.2 ± 0.1	EELS	This study
		579.6 ± 0.2	588.9 ± 0.2	XPS	Allen et al., 1973,[c] 1976
$PbCrO_4$	VI	578.6	587.2	XPS	Kendelewicz et al., 1999
		580.9	587.8–589.5	EELS	Brydson et al., 1993
Cs_2CrO_4	VI	579.8 ± 0.2	588.8 ± 0.2	XPS	Allen et al., 1973,[c] 1976
Li_2CrO_4	VI	579.8 ± 0.2	589.0 ± 0.2	XPS	Allen et al., 1973,[c] 1976
Na_2CrO_4	VI	579.8 ± 0.2	589.1 ± 0.2	XPS	Allen et al., 1973,[c] 1976

[a]As reported in reference as binding energies.

[b]Electron energy loss spectroscopy (EELS) L-edge onsets quoted in reference, however L-peak positions are shown here.

[c]After recalibrating the X-ray photoelectron spectroscopy (XPS), Au $4f_{7/2}$ line to 84.0 eV from 82.8 eV.

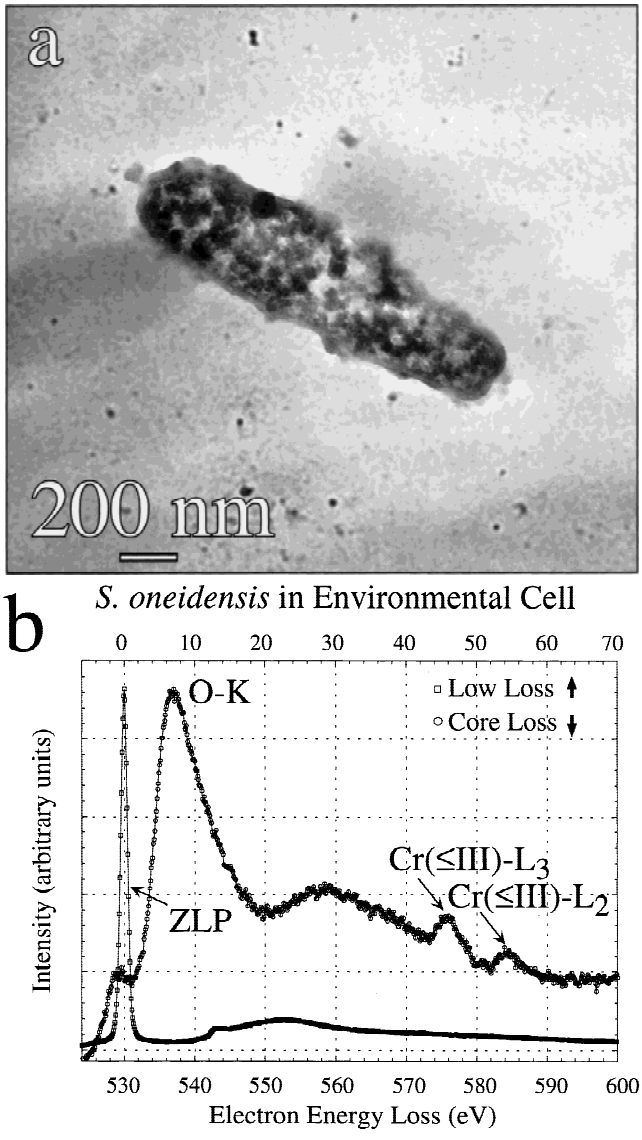

Figure 7. *S. oneidensis* in the EC at 100 Torr. **a:** Cell is encrusted/impregnated with electron dense particulates. **b:** EC-TEM electron energy loss spectroscopy (EELS) spectrum from the bacterium demonstrates the presence of Cr. Both the low-loss spectrum containing the zero-loss peak (ZLP) and the core-loss spectrum of the O-K and Cr-L absorption edges are shown. The ZLP represents electrons that have undergone elastic and quasi-elastic (mainly phonon) interactions. Its full width at half maximum is a measure of the instrumental resolution, which under these EC-TEM conditions is ≈1 eV. The top abscissa corresponds to the low-loss spectrum and the bottom abscissa corresponds to the core-loss spectrum.

the core-loss regime at 537.1 ± 0.5 eV arising from H_2O in the hydrated bacterium and its extracellular substances. A less intense feature at 529.2 ± 0.5 eV can be attributed to oxygen 2*p* hybridization with the Cr 3*d* band. The broad feature at 558 eV can be attributed to plural (O-K core-loss plus plasmon) scattering. However, the low-loss spectrum illustrates that multiple scattering is not severe. The total thickness traversed by the electron beam, estimated by the log-ratio technique (e.g., see Egerton, 1996), is 1.13 λ, where λ is the mean free path for inelastic scattering through the EC windows and specimen. The low-loss spectrum also exhibits a sharp feature at 13.2 eV that is only observed in EELS spectra collected in the EC. It is consistent with the K-edge of hydrogen (Geiger and Schmoranzer, 1969). Similar EELS edges at 13 eV have also been observed in frozen-hydrated specimens: cryosectioned liver and cryosectioned 6-molar glycerol solution containing 6% bovine serum albumin (Leapman and Sun, 1995). These energy loss edges were observed concurrently with electron-beam-induced bubble formation and were attributed to hydrogen formation presumably arising from reactions of radiolysis-formed free radicals with organic molecules. In that work, bubble formation was only observed in pure ice at much higher electron doses, suggesting in the absence of organic molecules there was a higher probability for recombination of hydrogen and hydroxyl radicals.

Clearly visible in the core-loss spectrum (Fig. 7) are Cr-$L_{2,3}$ edges, confirming the presence of Cr and suggesting the precipitates are Cr-rich. A comparison of core-loss spectrum from *S. oneidensis* and Cr standards of known oxidation state is shown in Figure 8. The spectrum of $KCr(SO_4)_2 \cdot 12H_2O$ exhibits a peak at 535.7 eV similar to the stronger feature observed in the spectrum from hydrated *S. oneidensis,* and likely corresponds to H_2O bound in the structure. The $L_{2,3}$ lines for the standards show a systematic chemical shift and variation in relative intensity with oxidation state. In addition, the $L_{2,3}$ lines of the K_2CrO_4 peaks appear asymmetric because each is split into two separate peaks separated by ~ 2eV.

Measurement of the L_3 peak positions is straightforward and the results for the Cr-standards are shown in Figure 9 and are summarized in Table 1. Table 1 includes published $L_{2,3}$ peak positions from previous EELS studies as well as core-level (or inner-shell) binding energies measured from X-ray photoelectron spectroscopy (XPS) studies. In XPS, a bulk specimen is illuminated with monochromatic X-rays and the kinetic energies of ejected photoelectrons are measured. In comparison, EELS measures the energy loss of electrons that travel through a specimen. The EELS edge onset, the sudden rise in intensity preceding each of the $L_{2,3}$ peaks, represents the ionization threshold which approximately corresponds to the inner-shell binding en-

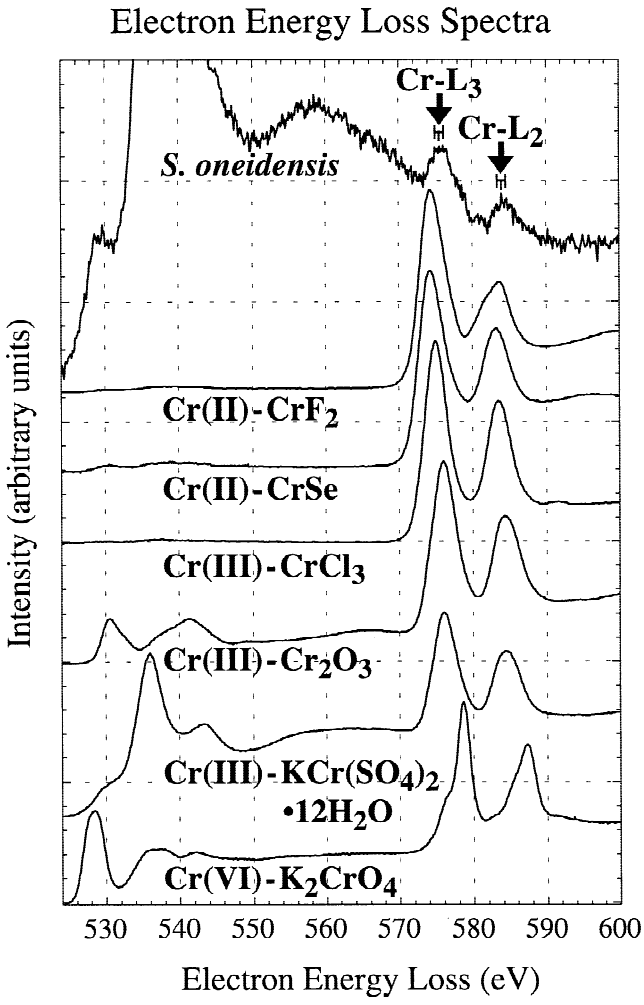

Figure 8. A comparison of the core-loss EELS spectra of encrusted *S. oneidensis* in the EC at 100 Torr and Cr standards of known oxidation state. Spectra were normalized to the intensity of the L_3 peak and offset from one another. The spectra shown for the Cr standards represent the sum of the 20 individual spectra acquired. The error bars shown for *S. oneidensis* represent the error in energy loss calibration for that spectrum only. For the errors associated with the other spectra, see Table 1.

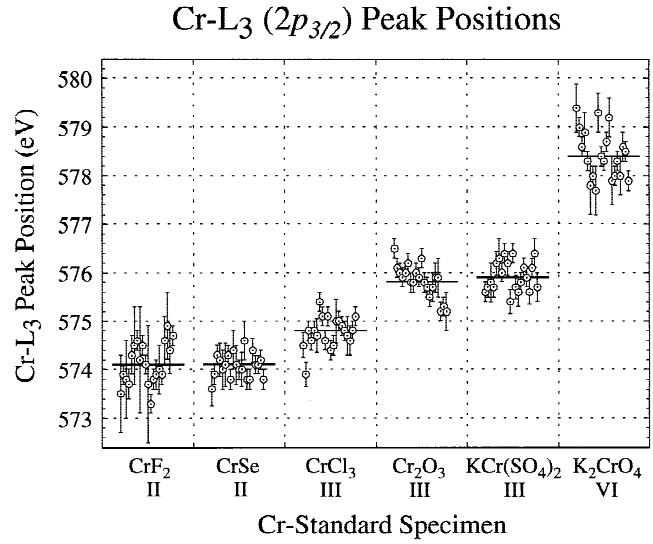

Figure 9. The measured L_3 peak positions for the Cr oxidation-state standards. The error bars for the data points represent the measured drift in the EELS spectrometer during acquisition. The bar represents the mean of the measured values. The Roman numerals along the abscissa indicate the formal valence state of Cr in the standard.

ergy. The difference in chemical shift measured by EELS and XPS for oxides has been suggested to be on the order of the band-gap energy (Leapman et al., 1982). Furthermore, it has been argued that many-body relaxation effects, where nearby electron orbitals are pulled towards a core hole, may be less in EELS than in XPS (Egerton, 1996). This could contribute to differences in spectra measured by the two techniques. However, Table 1 shows that the scatter in the reported EELS measurements fall within that of XPS measurements. The EELS core-loss spectrum from *S. oneidensis* (Figs. 7, 8) has a relatively strong Cr-L_3 peak at 575.7 ± 0.5 eV (together with its associated Cr-L_2 peak at 584.5 ± 0.5 eV). The Cr-L_3 peak is consistent with a highly reduced form of Cr with oxidation state +3 or lower (see Table 1).

To measure Cr oxidation state using the ratio of L_3/L_2 integrated-peak intensities, two methods of background subtraction were used. The first method, illustrated in Figure 10, is similar to the double step function used by Pearson et al. (1993). In this method, the Cr-L_3 pre-absorption edge was fit to a power law and subtracted. A linear function was then fit to the Cr-L_2 post-edge region over a 20 eV window (extending from 600 to 620 eV). Typically, background windows are chosen between 50–100 eV because smaller windows are susceptible to plural scattering effects. However, there were insufficient channels in the data to use a larger window since the O-K edge region was included. The fitted background was extrapolated into the L_2 threshold region. A linear step function was inserted at the L_2 maximum and a straight line (of the same slope as that fitted to the Cr-L_2 post-edge region) was extrapolated into the L_3 threshold. A second step function was inserted at the L_3 maximum and set to zero below the L_3 maximum. The ratio for the step heights was set at 2:1, consistent with the multiplicity of the initial states, that of four $2p_{3/2}$ electrons

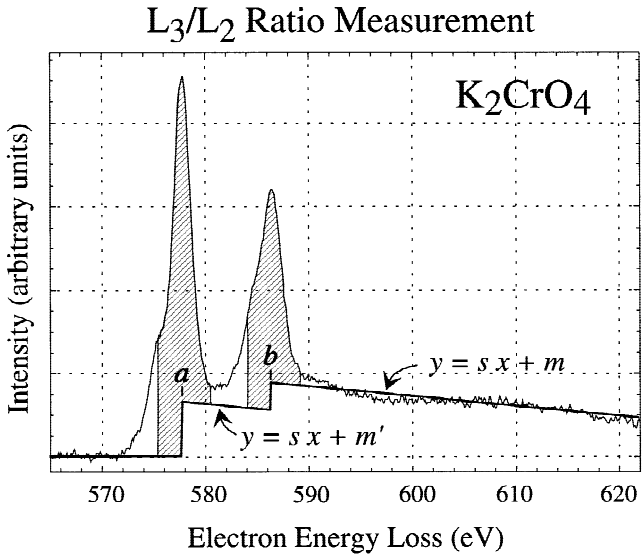

Figure 10. Core-loss EELS spectrum for K_2CrO_4 illustrating the background subtraction used in method I. The step function (bold line) used to subtract the background from the $L_{2,3}$ edges and the areas integrated to yield peak intensities (shaded regions) are shown. The fitting parameters *a, b, s,* and *m* are: the L_3 maximum, the L_2 maximum, the slope of the linear function fitted to the 20 eV post-L_2-edge region (600–620 eV), and the intercept of the linear function. The parameter m' is given by $m' = (2m - as)/3$.

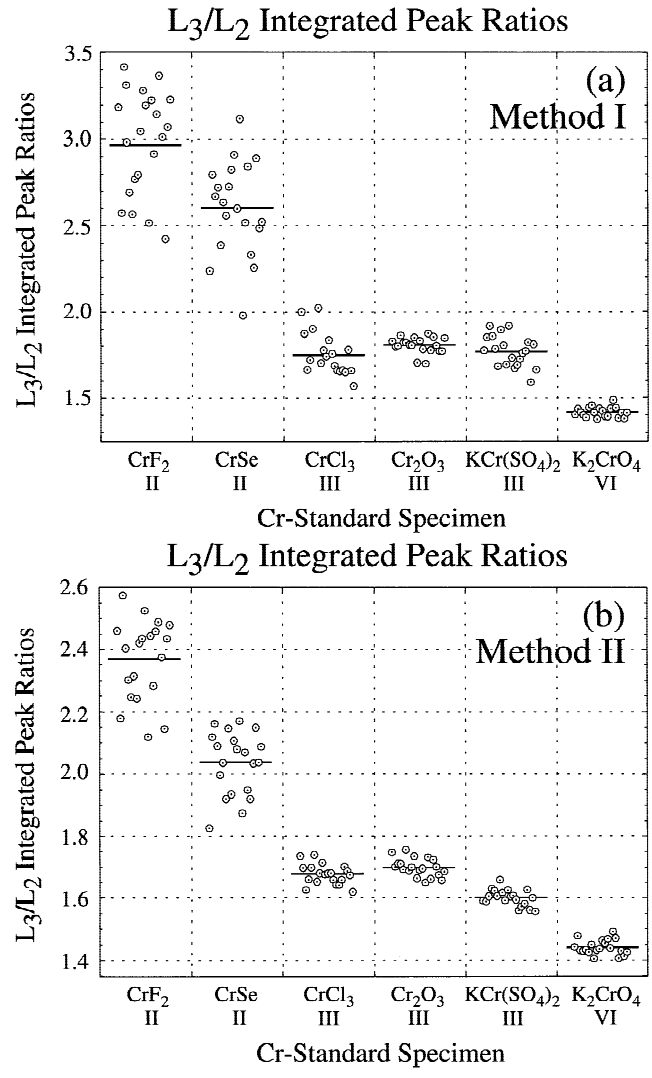

Figure 11. The measured L_3/L_2 integrated-peak intensity ratios for the Cr oxidation-state standards: background subtraction method I **(a),** and background subtraction method II **(b).** The bar represents the mean of the measured values. There is no straightforward method to determine experimental errors for the individual measurements, so none are reported. The Roman numerals along the abscissa indicate the formal valence state of Cr in the standard.

and two $2p_{1/2}$ electrons. It should be noted that the ratios of L_3 to L_2 intensities do not follow the expected 2:1 ratio for early 3*d* transition metals (Leapman and Grunes, 1980). These anomalous ratios can be partially explained by atomic multiplet effects producing overlapping transitions from $2p_{3/2}$ and $2p_{1/2}$ states (Zaanen et al., 1985). Nonetheless, an approximation of 2:1 is sufficient for this work.

Although the first subtraction method approximates the decreasing background, the fit of Cr-L_2 post-edge region was often affected by a broad post-edge feature, containing plural scattering effects not completely removed from the spectra. The post-edge feature varied with each spectrum, introducing scatter in the L_3/L_2 peak ratio measurements. To provide a more consistent background subtraction for all spectra, a second method using a flat, two-step function was applied. As before, the Cr-L_3 pre-absorption edge was fit to a power-law and subtracted. A linear function of slope zero was fit to a 2-eV-wide window immediately following the Cr-L_2 peak prior to the post-edge feature. The fitted background was extrapolated into the L_2 threshold region. A linear step function was inserted at the L_2 maximum and a straight line was extrapolated into the L_3 threshold. A second step function was inserted at the L_3 maximum and set to zero below the L_3 maximum. The ratio of the step heights was set to 2:1, as before.

Once the background was subtracted using either of the two methods, the Cr-L peaks were integrated over a 5-eV window. The L_3/L_2 peak ratios for the Cr-standards are shown in Figure 11 and summarized in Table 2. The flat, two-step background subtraction method yielded lower values, however, less relative scatter in the data. The core-loss spectra for K_2CrO_4 exhibited almost no post-L_2-edge fea-

Table 2. Cr-L Adsorption Edge Ratios

		L_3/L_2 for two background subtraction methods	
Compound	Formal valence	Method I, Pearson et al. (1993)	Method II, flat two-step
CrF_2	II	2.97 ± 0.07	2.37 ± 0.03
CrSe	II	2.60 ± 0.06	2.04 ± 0.02
$CrCl_3$	III	1.75 ± 0.03	1.68 ± 0.01
Cr_2O_3	III	1.81 ± 0.01	1.70 ± 0.01
$KCr(SO_4)_2 \cdot 12H_2O$	III	1.77 ± 0.02	1.60 ± 0.01
K_2CrO_4	VI	1.42 ± 0.01	1.44 ± 0.01

tures and this may account for the close similarity in L_3/L_2 peak ratios determined using the two background subtraction methods. In comparison, the L_3/L_2 peak ratio measured for the precipitates associated with *S. oneidensis,* 2.75 ± 0.30 (background method I) and 1.90 ± 0.30 (background method II), is consistent with a Cr oxidation state of +3 or lower.

The correlation between measured L_3/L_2 integrated-peak intensity ratios and L_3 peak positions for the Cr oxidation-state standards is shown in Figure 12. Measurements of the standards demonstrate that Cr oxidation states fall within well-separated regions in the correlation plot. Within a given oxidation state, spectra for the individual standards fall within separate groupings reflecting possible differences in atom coordination, spin-orbit interactions, and crystal field splitting. The correlation plot indicates that reduced Cr associated with *S. oneidensis* is most consistent with oxidation state +3.

Strong direct evidence indicating that the bacteria are the active sites of Cr(VI) reduction is provided by the EELS spectra. Measurements of both the chemical shift in L_3 peak position and the ratio of L_3/L_2 integrated-peak intensities of encrusted bacteria indicate the presence of Cr in oxidation state +3 or lower. The population of *S. oneidensis* which exhibits low contrast in bright field imaging in the EC (see Figs. 5a,c) might correspond to younger generations of bacteria which grew in a detoxified environment having much lower CrO_4^{2-} ion concentrations than present during previous generations. Furthermore, this population could contain mutants resistant to Cr(VI) toxicity. Mutations can arise from DNA damage by cellular interactions with Cr(VI) in their parent cells. Chromosomal mutations which inhibit transport of Cr(VI) are believed to be responsible for Cr(VI) resistance (Cervantes and Silver, 1992). Loss of the Cr(VI) transport function by mutant cells could inhibit Cr(VI) reduction, and consequently, bioaccumulation of reduction products.

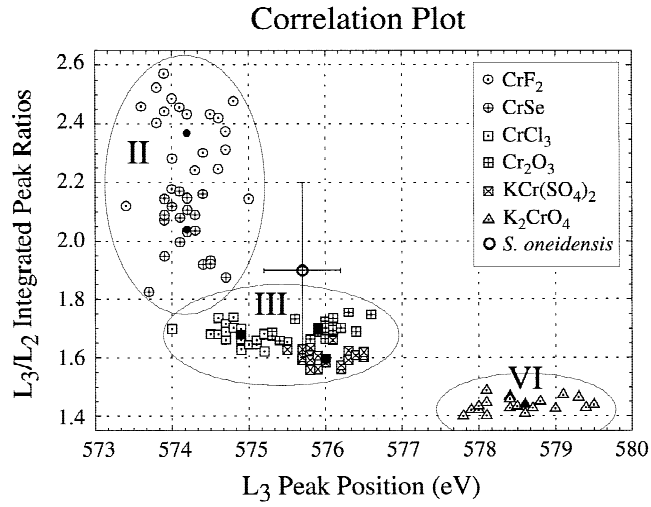

Figure 12. The correlation between measured L_3/L_2 integrated-peak intensity ratios and L_3 peak positions for the Cr oxidation-state standards. The plotted L_3/L_2 ratios were determined using background subtraction method II. The different Cr oxidation states fall within separate regions in the plot and are labeled II, III, and VI. The solid data points represent the mean of the data for a particular Cr standard. The open circle with error bars represents the measurement of encrusted *S. oneidensis.*

Summary

The biological reduction of Cr(VI) by the facultative anaerobe *Shewanella oneidensis* was examined. In situ EC-TEM was used to observe hydrated bacteria sampled from 51-day cultures (examined by EC-TEM after 53 days of initial inoculation of culture). Chemical and oxidation state infor-

mation was acquired with high spatial resolution using EELS. Two distinct populations were observed: bacteria that exhibit low image contrast and bacteria that are encrusted with precipitates (containing Cr of oxidation state +3 or lower) that formed as products of microbial Cr(VI) reduction. Microanalysis suggests that *S. oneidensis* can sequester Cr(VI) from its environment by reduction to insoluble forms. These results demonstrate the capability to determine the valence state of Cr in association with hydrated bacteria in an environmental cell transmission electron microscope.

Acknowledgments

This work was performed under ONR program element 0602233N and ONR-ASEE Postdoctoral Fellowship Program (K. Lowe). We thank Dr. K. Nealson (NASA Jet Propulsion Laboratory, Pasedena, CA) for kindly providing specimens of *S. oneidensis.* We thank Richard Ray (NRL) for ESEM imaging. We also thank Dr. R.K. Pope (Southampton College, Division of Natural Science) for valuable discussions.

References

Allen GC, Tucker PM (1976) Multiplet splitting of X-ray photoelectron lines of chromium complexes—effect of covalency on 2*p* core level spin-orbit separation. *Inorg Chim Acta* 16:41–45

Allen GC, Curtis MT, Hooper AJ, Tucker PM (1973) X-ray photoelectron spectroscopy of chromium-oxygen systems. *J Chem Soc, Dalton Trans* 16:1675–1683

Asami K, Hashimoto K (1977) X-ray photoelectron-spectra of several oxides of iron and chromium. *Corros Sci* 17:559–570

Baes CF, Mesmer RE (1976) *The Hydrolysis of Cations.* New York: John Wiley & Sons

Barlett RJ, James BR (1988) Mobility and bioavailability of chromium in soils. In: *Chromium in the Natural and Human Environments,* Nriagu J, Nieboer E (eds). New York: John Wiley & Sons, pp 267–304

Brito F, Ascanio J, Mateo S, Hernández C, Araujo L, Gili P, Martín-Zarza P, Domínguez S, Mederos A (1997) Equilibria of chromate(VI) species in acid medium and ab initio studies of these species. *Polyhedron* 16:3835–3846

Brydson R, Garvie LAJ, Craven AJ, Sauer H, Hofer F, Cressey G (1993) $L_{2,3}$ edges of tetrahedrally coordinated d^0 transition-metal oxyanions XO_4^{n-}. *J Phys: Condens Matter* 5:9379–9392

Cervantes C, Silver S (1992) Plasmid chromate resistance and chromate reduction. *Plasmid* 27:65–71

Characklis WG, Marshall KC (1990) *Biofilms.* Toronto: John Wiley & Sons

Cieslak-Golonka M (1991) Spectroscopy of chromium(VI) species. *Coord Chem Rev* 109:223–249

Cieslak-Golonka M (1995) Toxic and mutagenic effects of chromium(VI). A review. *Polyhedron* 15:3667–3689

Clesceri LS, Greenberg AE, Eaton AD (eds) (1999) *Standard Methods for the Examination of Water and Wastewater.* Washington, DC: American Public Health Association

Cranston RE, Murray JW (1980) Chromium species in the Columbia River and estuary. *Limnol Oceanogr* 25:1104–1112

Cressey G, Henderson CMB, van der Laan G (1993) Use of L-edge X-ray absorption spectroscopy to characterize multiple valence states of 3*d* transition metals; a new probe for mineralogical and geochemical research. *Phys Chem Miner* 20:111–119

Decho AW (2000) Microbial biofilms in intertidal systems: an overview. *Contin Shelf Res* 20:1257–1273

Deng B, Stone AT (1996a) Surface-catalyzed chromium(VI) reduction: reactivity comparisons of different organic reductants and different oxide surfaces. *Environ Sci Technol* 30:2484–2494

Deng B, Stone AT (1996b) Surface-catalyzed chromium(VI) reduction: the TiO_2-Cr^{VI}-Mandelic acid system. *Environ Sci Technol* 30:463–472

Dubois F, Belleville F (1991) Chromium-physiological-role and implications for human-disease. *Pathol Biol* 39:801–808

Egerton RF (1996) *Electron Energy-loss Spectroscopy in the Electron Microscope.* New York: Plenum

Egerton RF, Yang YY, Chen FYY (1991) EELS of "thick" specimens. *Ultramicroscopy* 38:349–352

Fendorf S, Wielinga BW, Hansel CM (2000) Chromium transformations in natural environments: the role of biological and abiological processes in chromium(VI) reduction. *Int Geol Rev* 42:691–701

Fink J, Müller-Heinzerling T, Scheerer B, Speier W, Hillebrecht FU, Fuggle JC, Zaanen J, Sawatzky GA (1985) 2*p* absorption spectra of the 3*d* elements. *Phys Rev B* 32:4899–4904

Fude L, Harris B, Urrutia MM, Beveridge TJ (1994) Reduction of Cr(VI) by a consortium of sulfate-reducing bacteria (SRB-III). *Appl Environ Microbiol* 60:1525–1531

Fukami A, Fukushima K, Kohyama N (1991) Observation technique for wet clay minerals using film-sealed environmental cell equipment attached to high-resolution electron microscope. In:

Microstructure of Fine-grained Sediments from Mud to Shale, Bennett RH, Bryant WR, Hulbert MH (eds). New York: Springer-Verlag, pp 321–331

Geiger J, Schmoranzer H (1969) Electronic and vibrational transition probabilities of isotopic hydrogen molecules H_2, HD and D_2 based on electron energy loss spectra. *J Mol Spectrosc* 32:39–53

Hamilton JH, Wetterhahn KE (1987) *Handbook on Toxicity of Inorganic Compounds,* Seiler HG, Sigel H (eds). New York: Marcel Dekker

Hill RRH, Cowley HM (1986) Bacterial bioabsorption of chromium from industrial cooling water. *S Afr J Sci* 82:595–596

Holdway DA (1988) The toxicity of chromium to fish. In: *Chromium in the Natural and Human Environments,* Nriagu JO, Nieboer E (eds). New York: John Wiley & Sons, pp 369–398

Ikemoto I, Ishii K, Kinoshita S, Kuroda H, Franco MA, Thomas JM (1976) X-ray photoelectron spectroscopic studies of CrO_2 and some related chromium compounds. *J Solid State Chem* 17:425–430

Katz SA (1991) The analytical biochemistry of chromium. *Environ Health Persp* 92:13–16

Kendelewicz T, Liu P, Doyle CS, Brown GE, Nelson EJ, Chambers SA (1999) X-ray absorption and photoemission study of the absorption of aqueous Cr(VI) on single crystal hematite and magnetite surfaces. *Surf Sci* 424:219–231

Konno H, Tachikawa H, Furusaki A, Furuichi R (1992) Characterization of lanthanum(III) chromium(V) tetraoxide by X-ray photoelectron spectroscopy. *Anal Sci* 8:641–646

Krishnan KM (1990) Iron $L_{3,2}$ near-edge fine structure studies. *Ultramicroscopy* 32:309–311

Krivanek OL, Paterson JH (1990) ELNES of 3*d* transition-metal oxides I. Variations across the periodic table. *Ultramicroscopy* 32: 313–318

Ku Y, Jung I (2001) Photocatalytic reduction of Cr(VI) in aqueous solutions by UV irradiation with the presence of titanium dioxide. *Wat Res* 35:135–142

Leapman RD, Grunes LA (1980) Anomalous L_3/L_2 white-line ratios in the 3*d* transition metals. *Phys Rev Lett* 45:397–401

Leapman RD, Sun S (1995) Cryo-electron energy loss spectroscopy: observations on vitrified hydrated specimens and radiation damage. Ultramicroscopy 59:71–79

Leapman RD, Grunes LA, Fejes PL (1982) Study of the L_{23} edges in the 3*d* transition metals and their oxides by electron-energy-loss spectroscopy with comparisons to theory. *Phys Rev B* 26:614–635

Lee JV, Gibson DM, Shewan JM (1977) A numerical taxonomic study of some *Pseudomonas*-like marine bacteria. *J Gen Microbiol* 98:439–451

Little BJ, Wagner P, Ray R, Pope R, Scheetz R (1991) Biofilms—an ESEM evaluation of artifacts introduced during SEM preparation. *J Indust Microbiol* 8:213–222

Lovley DR (1993) Dissimilatory metal reduction. *Annu Rev Microbiol* 47:263–290

Lovley DR, Phillips EJP, Gorby YA, Landa ER (1991) Microbial reduction of uranium. *Nature* 350:413–416

Lytle CM, Lytle FW, Yang N, Qian JH, Hansen D, Zayed A, Terry N (1998) Reduction of Cr(VI) to Cr(III) by wetland plants: potential for in situ heavy metal detoxification. *Environ Sci Technol* 32:3087–3093

MacDonell MT, Colwell RR (1985) Phylogeny of the *Vibrionaceae,* and recommendation for two new genera, *Listonella* and *Shewanella. Syst Appl Microbiol* 6:171–182

Marques AM, Tomas MJE, Congregado F, Simon-Pujol MD (1982) Accumulation of chromium by *Pseudomonas aeruginosa. Microbios Lett* 21:143–147

Moffat TP, Latanision RM, Ruf RR (1995) An X-ray photoelectron spectroscopy study of chromium-metalloid alloys-III. *Electrochim Acta* 40:1723–1734

Mugo RK, Orians KJ (1993) Seagoing method for the determination of chromium(III) and total chromium in sea-water by electron-capture detection gas chromatography. *Anal Chim Acta* 271: 1–9

Myers CR, Nealson KH (1988a) Bacterial manganese reduction and growth with manganese oxide as the sole electron-acceptor. *Science* 240:1319–1321

Myers CR, Nealson KH (1988b) Microbial reduction of manganese oxides: interactions with iron and sulfur. *Geochim Cosmochim Acta* 52:2727–2732

Ohtake H, Fujii E, Kiyishi T (1990) Bacterial reduction of hexavalent chromium: kinetic aspects of chromate reduction by *Enterobacter cloacae* HO. *Biocatalysis* 4:227–235

Paterson JH, Krivanek OL (1990) ELNES of 3*d* transition-metal oxides II. Variations with oxidation-state and crystal-structure. *Ultramicroscopy* 32:319–325

Pearson DH, Ahn CC, Fultz B (1993) White lines and *d*-electron occupancies for the 3*d* and 4*d* transition metals. *Phys Rev B* 47: 8471–8478

Pettine M, Millero FJ, Passino R (1994) Reduction of chromium (VI) with hydrogen sulfide in NaCl media. *Marine Chem* 46:335–344

Pettine M, Barra I, Campanella L, Millero FJ (1998a) Effect of metals on the reduction of chromium (VI) with hydrogen sulfide. *Wat Res* 32:2807–2813

Pettine M, D'Ottone L, Campanella L, Millero FJ, Passino R (1998b) The reduction of chromium (VI) by iron (II) in aqueous solutions. *Geochim Cosmochim Acta* 62:1509–1519

Rai D, Sass BM, Moore DA (1987) Chromium(III) hydrolysis constants and solubility of chromium(III) hydroxide. *Inorg Chem* 26:345–349

Sedlak DL, Chan PG (1997) Reduction of hexavalent chromium by ferrous iron. *Geochim Cosmochim Acta* 61:2185–2192

Sugi H, Akimoto T, Sutoh K, Chaen S, Oishi N, Suzuki S (1997) Dynamic electron microscopy of ATP-induced myosin head movement in living muscle thick filaments. *Proc Natl Acad Sci USA* 94:4378–4382

Tandon RK, Crisp PC, Ellis J, Baker RS (1984) Effect of pH on chromium(VI) species in solution. *Talanta* 31:227–228

van Aken PA, Liebscher B, Styrsa VJ (1998) Quantitative determination of iron oxidation states in minerals using Fe $L_{2,3}$-edge electron energy-loss near-edge structure spectroscopy. *Phys Chem Miner* 25:323–327

Vandevivere P, Kirchman DL (1993) Attachment stimulates exopolysaccharide synthesis by a bacterium. *Appl Environ Microbiol* 59:3280–3286

Venkateswaran K, Moser DP, Dollhopf ME, Lies DP, Saffarini DA, MacGregor BJ, Ringelberg DB, White DC, Nishijima M, Sano H, Burghardt J, Stackebrandt E, Nealson KH (1999) Polyphasic taxonomy of the genus *Shewanella* and description of *Shewanella oneidensis* sp. nov. *Int J Syst Bacteriol* 49:705–724

Wang YT, Shen H (1997) Modeling Cr(VI) reduction by pure bacterial cultures. *Wat Res* 31:727–732

Wang ZL, Bentley J, Evans ND (1999) Mapping the valence states of transition-metal elements using energy-filtered transmission electron microscopy. *J Phys Chem B* 103:751–753

Zaanen J, Sawatzky GA (1986) Strong interference between decay channels and valence-electron rearrangements in core-hole spectroscopy. *Phys Rev B* 33:8074–8083

Zaanen J, Sawatzky GA, Fink J, Speier W, Fuggle JC (1985) $L_{2,3}$ absorption-spectra of the lighter 3*d* transition-metals. *Phys Rev B* 32:4905–4913

Zachara JM, Girvin DC, Schmidt RL, Resch CT (1987) Chromate adsorption on amorphous iron oxyhydroxide in the presence of major groundwater ions. *Environ Sci Technol* 21:589–594